

PALEO-ICE THICKNESS OF A GLACIOVOLCANIC TINDAR RIDGE, REYKJANES PENINSULA, SOUTHWEST ICELAND

CHLOE WALLACE, The College of Wooster
Research Advisor: Meagen Pollock

INTRODUCTION

When fluid magma erupts under ice or in water during an effusive eruption, pillow lava is produced (Thordarson and Hoskuldsson, 2002). The most important characteristic of pillows for this study is the glassy rind that forms on the outside edge due to the rapid quenching process that takes place during emplacement when lava interacts with water (Fig. 1). The glassy rinds are used to extrapolate information about the environment present during eruption based on the content of volatiles, specifically H_2O (von Aulock et al., 2014). This is possible because magma degassing serves as a function of the confining pressure that existed when the lava was erupted (Tuffen et al., 2010).

Different volatile species have different solubilities during magma degassing due to pressure, magma composition, and the concentration of other volatile species present. H_2O has a higher solubility in basaltic lavas than other volatiles. For this reason, the water concentration in basaltic glass can be measured using Fourier Transform Infrared Spectroscopy (FTIR) far easier than other volatiles (Tuffen et al., 2010). If magma composition and volatile concentrations are known, then concentrations of H_2O within melts are a function of the pressure experienced at the time of eruption. Thus, the process of magma degassing makes it possible to extrapolate approximate paleo-ice thickness from volcanic glasses. In order for the dissolved volatile content remaining in the sample to record confining pressure, degassing must have occurred. Vesicles within the sample indicate that degassing has taken place (Fig. 1).

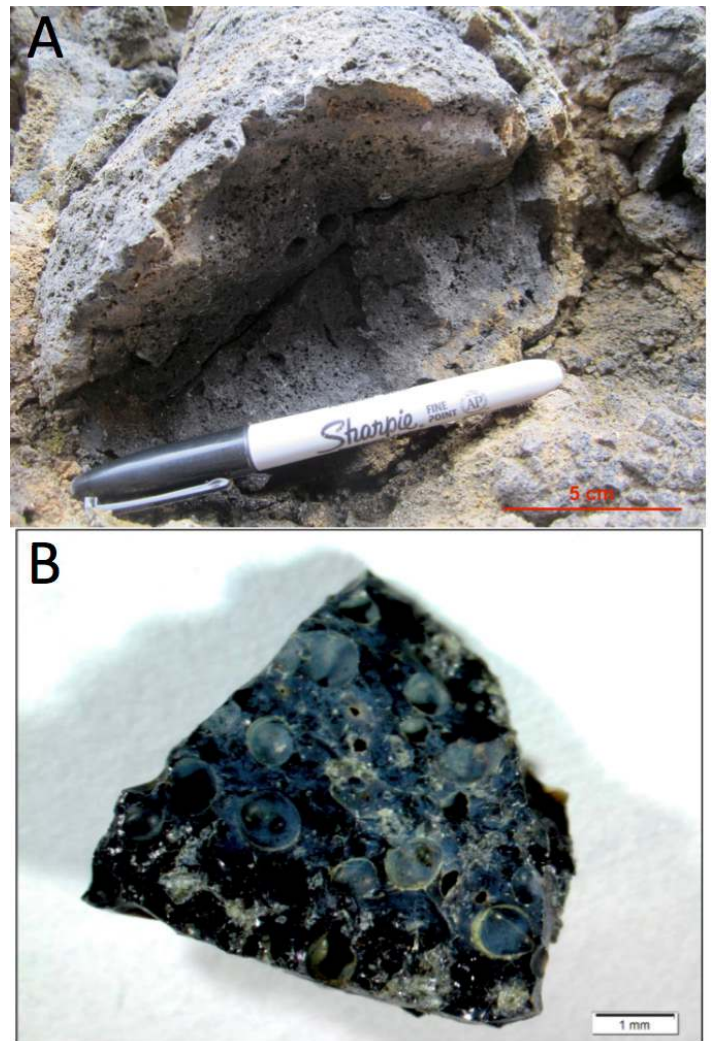


Figure 1. A: Pillow 16CW02 collected at the base of the gully near Vatnsskard quarry; around the edge is the quenched pillow glass. B: An example of a glass chip before polishing; note the many vesicles present (Hiatt, 2014).

This project presents an analysis of vesiculated glassy pillow rinds from a tindar ridge (Undirhlídar ridge) as a method of understanding past glacial extent and behavior during the late Weichselian. Using whole-rock analysis methods including X-ray Fluorescence and Electron-probe (EPMA), along with FTIR analysis of volatiles, a story can be developed that describes how the varying paleo-ice thicknesses across the ~4 km ridge affected the ridge's emplacement during eruption. As more studies are conducted on subglacial eruptions, the knowledge of their complexity grows, and this study demonstrates the same.

METHODS

Two sample types were collected in the field: glass and whole-rock. Glass samples were collected for volatile concentration and geochemical analyses by FTIR and electron-probe (EPMA), respectively. Whole-rock samples were collected for X-ray Fluorescence (XRF) geochemical analysis. Thirteen (twelve with a corresponding elevation) quenched rind glass samples were taken along the ridge, with a whole rock sample collected to correspond to each (Fig. 2). Three samples were collected within Undirhlídar quarry (Fig. 2, pink triangles), two samples were collected within Vatnsskard quarry (blue triangles), two samples were collected within the same erosional gully separated by 73 m (purple triangles), five samples were collected at various locations along the ridge running between the two quarries (red triangles), and a final sample (16BRE07) was collected at the top of a gully near Undirhlídar without an elevation, so it is not included on the sample map.

All 13 glass samples collected for FTIR analysis have a corresponding whole-rock sample for XRF analysis of the pillow geochemistry. Preparation of whole-rock samples entails making powders, fused beads and pressed pellets, which are analyzed for major and minor element geochemistry by XRF at The College of Wooster. Whole-rock powders were sent to Washington State University for Inductively Coupled Plasma Mass Spectrometry (ICP-MS) analysis. A Cameca SX50 Electron Microprobe was used at the University of Massachusetts at Amherst to analyze geochemistry of the glass chips themselves.

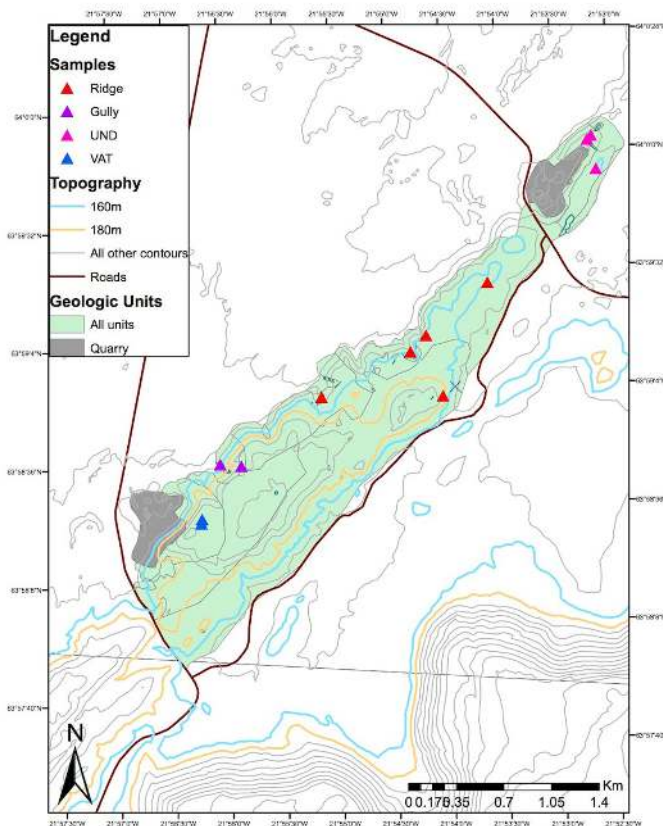


Figure 2. Sample map showing the two quarries, the location of all twelve samples, major roads, and topography, specifically the highlighted contour zone between 160 m (blue) and 180 m (orange).

Glass preparation follows a ‘doubly polished’ method developed by Alex Hiatt (2014). The glass samples are analyzed at the University of Massachusetts at Amherst using a Bruker Tensor 27 FTIR with attached Hyperion 3000 microscope. Due to the process of magma degassing during eruption and the rapid quenching process that takes place when magma comes in contact with an aqueous environment, volatiles are trapped in a glassy rind that forms around the edge of pillows and can be measured for concentration using FTIR. FTIR produces a spectrum that shows peak height and peak position for total dissolved H₂O (OH species at ~3530 cm⁻¹). The peak height represents the absorption value and is used in conjunction with the molecular weight of water (18.02 g), the thickness of each polished glass wafer, the density of basalt glass (2750 g/liter), and an absorption coefficient (63 mol/cm) to extrapolate a water concentration in weight percent (Equation 1) (von

Aulock et al., 2014). The Beer-Lambert law allows for this relation of absorbance to total weight percent H₂O concentration:

$$\text{Equation 1: } c = (\text{m.w.} \times \text{abs.}) / (\rho \times d \times \epsilon)$$

Equation 1: *c* is wt. % H₂O concentration, *m.w.* is the molecular weight of water (18.02 g), *abs* is the absorption value, ρ is the density of basalt glass (2750 g/liter), *d* is the thickness of each polished wafer (microns), and ϵ is the absorption coefficient of 63 mol/cm (Dixon et al., 2002).

Rhyolite-MELTS is a web-based application that outputs liquidus temperature using the geochemical compositions and mean weight percent water concentration of each sample (Ghiorso and Sack, 1995). The geochemical composition of the samples gathered through EPMA represents the liquid composition most accurately, but some samples only have XRF geochemistry (16CW03 and 16MP06). The parameters used within the program are a starting temperature of 1200°C and a starting pressure of 2,000 bars. VolatileCalc is a program that outputs emplacement pressure in bars (Newman and Lowenstern, 2002). It requires four variables including the derived H₂O concentration from FTIR analysis (wt. %), major element geochemical data, specifically SiO₂ concentration (wt. %) derived from EPMA or XRF analyses, liquidus temperature derived from rhyolite-MELTS using EPMA or XRF geochemistry data, and standard CO₂ concentrations (minimum: 0 ppm and maximum: 25 ppm). The pressure value is converted from bars to megapascals (Mpa) by multiplying by 0.1, which allows the value to fit into an equation that calculates ice thickness and water depth in meters (Equation 2):

$$\text{Equation 2: } P = \rho \times g \times h$$

Equation 2: *P* is the hydrostatic/glaciostatic pressure (kg/cm²), ρ is density of ice/water (ice: 0.917 kg/m³; water: 0.1 kg/m³), *g* is acceleration due to gravity (9.8 m/s²), and *h* is the height of the column of liquid (m).

RESULTS

Table 1 represents the paleo-water data for all thirteen glass samples collected including mean H₂O concentration (wt. %), emplacement pressure at both

Sample Number	Sample Elevation (m)	Liquidus Temp. (°C)	Wt. % H ₂ O	Wt. % CO ₂	P (MPa)	Water Depth (m)	Ice Thick. (m)	Min. Ice Elevation (m)
16CW01	169	1219	0.28	0	0.9	92	100	269
				25	4.5	459	501	670
16CW02	148	1194	0.19	0	0.4	41	45	192
				25	4.2	429	467	615
16CW03	169	1218	0.16	0	0.3	31	33	203
				25	4.4	449	490	659
16CW04	161	1196	0.22	0	0.5	51	56	217
				25	6.0	612	668	829
16CW05	153	1212	0.23	0	0.6	61	67	220
				25	5.0	510	556	709
16CW07	196	1177	0.33	0	1.2	122	134	330
				25	5.6	571	623	819
16CW08	126	1179	0.29	0	0.9	92	100	226
				25	6.4	653	712	838
16CW09	221	1196	0.23	0	0.6	61	67	288
				25	4.5	459	501	722
16MP04	158	1197	0.16	0	0.3	31	33	191
				25	4.4	449	490	648
16MP06	147	1207	0.22	0	0.6	61	67	214
				25	4.9	500	545	692
16MP13	171	1214	0.23	0	0.6	61	67	238
				25	3.9	398	434	605
16MP14	159	1190	0.25	0	0.7	71	78	237
				25	4.4	449	490	649
16BRE07	N/A	1213	0.29	0	1.0	102	111	N/A
				25	4.4	449	490	N/A

Table 1. Analyses of H₂O, estimated confining pressures, water depths, and ice thicknesses for thirteen glass samples collected in 2016.

0 ppm CO₂ and 25 ppm CO₂ (MPa), corresponding water depth (m), corresponding ice thickness (m), and a minimum ice elevation (m).

Figure 3 displays all thirty-five data points currently derived for this field site. It is a combination of work from Hiatt (2014), Wallace (2016), and the twelve samples with location data collected for this particular study. The data are represented through both wt. % water concentration and pressure (MPa) versus elevation (m). The hydrostatic curves represent the pressure the samples theoretically should experience and the water concentration they should display if the ridge were built in a static lake. Thus, samples should show a decrease in pressure with increased stratigraphic height. Samples at lower and intermediate elevations starting at 112 m until approximately 164 m fall along a trend of decreasing pressure/water concentration with increasing stratigraphic height. Concurrently, beginning at approximately 120 m until 169 m, some samples display smaller emplacement pressures/water concentrations (~seven samples) that are not in line with the trend. Samples at higher elevations from 165-221 m fall along a second trend of decreasing pressure/water concentration and increasing stratigraphic height.

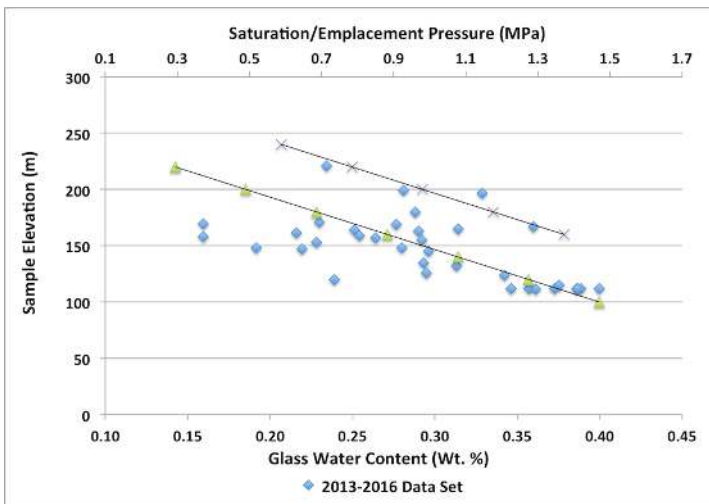


Figure 3. Graph of all thirty-five data points for paleo-water with calculated hydrostatic curves to explain subglacial eruption patterns. Green triangles represent hydrostatic conditions for a bedrock base at 100 m and an overlying water depth of 150 m. Purple Xs represent hydrostatic conditions for a bedrock at 160 m and an overlying water depth of 140 m.

DISCUSSION

Many of the samples at lower and intermediate elevations fall along the first hydrostatic curve (green triangles) from an elevation of 112-164 m. At the same time, a group of samples (approximately seven) plot below the first hydrostatic curve beginning at 120 m up to 169 m, meaning they were emplaced at lower pressures than expected under the hydrostatic conditions. Samples at higher elevations from 165-221 m fall along a second hydrostatic curve under similar conditions to the first curve. There is also an observable difference in emplacement pressure between samples collected from the core of the ridge versus the flank. Flanking pillows experience greater overlying pressure during emplacement, while core samples, which were emplaced first, experience less pressure. The model that best accounts for the majority of the samples is illustrated in Figure 4. It is different from past monogenetic models (Jones et al., 1969) and more complicated than a model calling for two separate eruptions. The model presented in Figure 4 introduces the idea of a fluctuating lake throughout the first eruption, both in regards to when core samples are erupted versus flank samples and especially as the first eruption nears the end. As the core of the ridge is being emplaced during the first eruption, the lake would have been at a particular level (Fig. 4A). As

more magma erupts, the ice would continue to melt and the lake level may have risen. This means as the flanking pillows were erupted, even at the same/similar elevations as the core samples, they would have experienced more pressure (Fig. 4B) (Russell et al., 2013). The group of samples that plot at lower pressures of the first hydrostatic curve represents the end of the first eruption and a lake that is not static. This is likely reflective of extensive melting and drainage events that are variable and common across the ridge (Fig. 4C). At this stage of the eruption, the thickness of the glacier largely varies across the ridge. The rest of the model is reflective of a second eruption, separate from the first eruption, in which ice conditions were able to reset to similar conditions as when the first eruption began (Fig. 4D). Based on the few samples available from the second eruption, the lake behavior cannot be fully determined. The lack of availability of samples from the second eruption is likely reflective of erosion. If there was a similar pattern of a fluctuating lake level as during the first eruption, there is currently no sample evidence of that.

The four-part model adds to the Pollock et al. (2014) model by incorporating paleo-water data. Pollock et al. (2014) proposed that two separate eruptions formed the quarry. The four-part model also supports this idea of two eruptions in order to build the entire length of the ridge. Paleo-water data suggests that the lake fluctuates as the ridge is built, causing a difference in the emplacement of core and flank samples. The paleo-water data also shows that there were likely drainage events that separated the two eruptions. This in turn, could have led to the emplacement of explosive, fragmental material, which has been identified in the quarry and presented in Pollock et al. (2014).

The highlighted contour lines in Figure 2 represent the area known as the “transition zone,” specifically between 160-180 m. It is in between these two contour lines that the differentiation between the two eruptions *most likely* exists. Elevation loosely correlates to volcanic stratigraphy, allowing us to make constraints on where the samples begin to differentiate between two separate eruptions. Based on the samples available, above 171 m seems to be indicative of the second eruption, and below 165 m seems to be indicative of the first eruption. The samples between

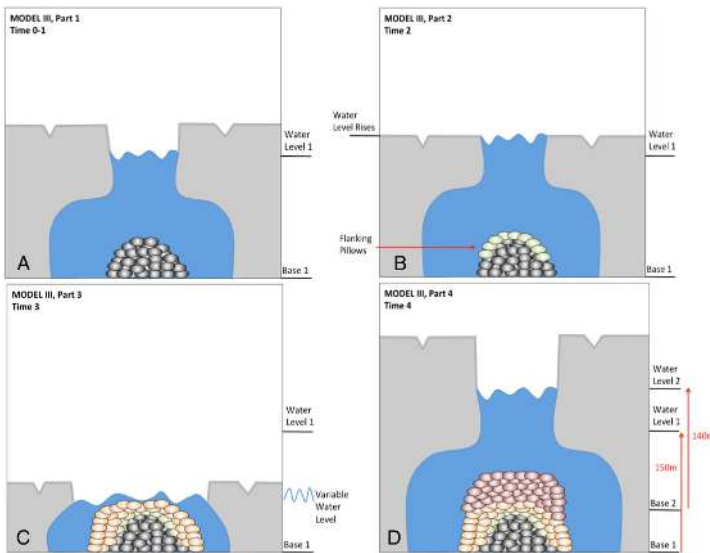


Figure 4. Best-fit model, which accounts for the most samples through a four-stage summation of the subglacial eruptive events that took place. A: Beginning of the first eruption, core samples emplaced under relatively static lake. B: Flank samples emplaced under more water due to ice melt; experiencing more pressure than core samples. C: Extensive ice melt nearing the end of the first eruption, leaving a variable lake level across the entirety of the ridge and causing variable drainage events. D: Some time interval after the first eruption persists in which the ice conditions reset to similar conditions as before the first eruption. The second eruption then takes place.

(165-171 m) can be either eruption, but all the samples currently analyzed except for one (VAT-NA-13-16; Hiatt, 2014) were emplaced during the first eruption. The two Vatnsskarð samples in blue (Fig. 2) are shown to be above the transition zone, but this is because the contour lines have not been updated to reflect new areas of the quarry that have been quarried since 2013, including this area where the two samples were collected.

Variations in water concentration and therefore emplacement pressure were the first line of evidence of different periods of pillow emplacement under different water/ice conditions. According to Edwards et al. (2009), “the 1996 Gjalp eruption in Iceland formed in the same location as a pre-existing glaciovolcanic ridge thought to have formed during an eruption in 1938.” This is evidence of the ability of multiple subglacial eruptions to take place within the same ridge. Additionally, based on the efficiency of heat transfer, there is enough heat produced during subglacial magmatic eruptions to melt a large amount

of overlying ice. For example, during the Gjalp 1996 eruption, it took less than 36 hours from the start of eruption to melt through ice at least 600 m thick (Gudmundsson et al., 2004; Edwards et al., 2009). The proximal eruption products of two modern basaltic glaciovolcanic eruptions, of Gjalp in 1996 and Grimsvotn in 1998, 2004, and 2011, are currently either relatively inaccessible or were covered within 1-2 years with snow and ice (Hungerford et al., 2014). This is evidence of the quick ability of these environments to reset, building ice back up to similar conditions that existed before an eruption began.

CONCLUSIONS

The best-fit model (Fig. 4) accounts for the majority of the samples. During the first eruption under a generally static lake, core samples were emplaced. As the eruption continued, flank samples were emplaced under greater pressure conditions (at least in the case of Vatnsskarð quarry) in response to the lake rising due to ice melt. The emplacement of pillows on the flanks of the pile versus within the core of the ridge explains samples at the same elevation as each other experiencing different pressures. Additionally, nearing the end of the eruption, extensive melting of the glacier had taken place, which caused fluctuating lake levels across the ridge, and variable drainage events throughout. This accounts for the a long-axis variability across the ridge illustrated through the samples. For this reason, the best-fit model introduces a fluctuating lake level, different from past models developed to explain subglacial eruptions. The transition zone seems to represent the differentiation between when the first and second eruption took place, with drainage events occurring between the two eruptions. It represents the age disparity that is illustrated through the samples, reflective of the time interval in which the ice conditions reset before the second eruption to similar conditions as when the first eruption began. When a second eruption did take place, the samples were emplaced at higher elevations, but under similar pressure conditions as samples much lower in elevation that correspond to the first eruption.

To conclude, the current data set of thirty-five points across the entire ridge and within the quarries presently illustrates that, based on where a sample falls

in elevation and where along the ridge it is located, an estimated emplacement pressure can be only *generally* assumed. Actual emplacement pressures account for a complexity that involves a long-axis variability across the ridge, core to flank variability, and age disparities. Subglacial eruptions are far more complex than previous monogenetic models propose. The work of Pollock et al. (2014) demonstrated this through geochemistry, and paleo-water data only confirms and adds to that complexity.

ACKNOWLEDGEMENTS

I would like to acknowledge the support of the Keck Geology Consortium, The National Science Foundation and ExxonMobil Corporation. Specifically, I would like to thank the NSF grant: NSF-REU1358987. Thank you to Henry J. Copeland Funding for the opportunity to travel to the University of Massachusetts at Amherst and Sheila Seaman for her help with FTIR and EPMA analyses. Lastly, thank you to the College of Wooster for supporting my conference travel.

REFERENCES

- Edwards, B.R., Skilling, I.P., Cameron, B., Haynes, C., Lloyd, A., and Hungerford, J.H.D., 2009, Evolution of an englacial volcanic ridge: Pillow Ridge tindar, Mount Edziza volcanic complex, NCVF, British Columbia, Canada: *Journal of Volcanology and Geothermal Research*, v. 185, p. 251-275.
- Ghiorso, M.S., and Sack, R.O., 1995, Chemical Mass Transfer in Magmatic Processes IV: A Revised and Internally Consistent Thermodynamic Model for the Interpolation and Extrapolation of Liquid-Solid Equilibria in Magmatic Systems at Elevated Temperatures and Pressures: *Contributions to Mineralogy and Petrology*, v. 119, p. 197-212.
- Gudmundsson, M.T., Sigmundsson, F., Björsson, H., Högnadóttir, T., 2004, The 1996 eruption at Gjalp, Vatnajökull ice cap, Iceland: efficiency of heat transfer, ice deformation and subglacial water pressure. *Bull Volcanology*, v. 66, i. 1, p. 46-65.
- Hiatt, Alexander R., 2014, Estimated Hydrostatic/Cryostatic Pressure During Emplacement of Pillow Lavas at Undirhlíðar Quarry, Reykjanes Peninsula, Southwest Iceland [Undergraduate thesis]: Wooster, The College of, 45 p.
- Hungerford, J.D.G., Edwards, B.R., Skilling, I.P., and Cameron, B.I., 2014, Evolution of a subglacial basaltic lava flow field: Tennena volcanic center, Mount Edziza volcanic complex, British Columbia, Canada: *Journal of Volcanology and Geothermal Research*, v. 272, p. 39-58.
- Jones, J.G., 1969, Intraglacial volcanoes of the Laugarvatn Region, Southwest Iceland: *Journal of the Geological Society of London*, v. 124, p. 197-211.
- Newman, S., and Lowenstern, J.B., 2002, VOLATILECALC: A silicate melt-H₂O-CO₂ solution model written in Visual Basic for excel: *Computers and Geosciences*, v. 28, i. 5, p. 597-604.
- Pollock, M., Edwards, B.R., Hauksdóttir, S., Alcorn, R., and Bowman, L., 2014, Geochemical and lithostratigraphic constraints on the formation of pillow-dominated tindars from Undirhlíðar quarry, Reykjanes Peninsula, Southwest Iceland: *Lithos*, v. 200-201, p. 317-333, doi:10.1016/j.lithos.2014.04.023.
- Russell, J. K., Edwards, B.R., and Porritt, L.A., 2013, Pyroclastic Passage Zones in Glaciovolcanic Sequences: *Nature Communications*, v. 4, i. 1788, p. 1-8.
- Thordarson, T., and Hoskuldsson, A., 2002, Iceland: England, Terra Publishing, 200 p.
- Tuffen, H., Owen, J., and Denton, J., 2010, Magma degassing during subglacial eruptions and its use to reconstruct palaeo-ice thicknesses: *Earth-Science Reviews*, v. 99, p. 1-18.
- von Aulock, F.W., Kennedy, B.M., Schipper, C.I., Castro, J.M., Martin, D.E., Oze, C., Watkins, J.M., Wallace, P.J., Puskar, L., Bégué, F., Nichols, A.R.L., and Tuffen, H., 2014, Advances in Fourier transform infrared spectroscopy of natural glasses: From sample preparation to data analysis: *Lithos*, v. 206-207, p. 52-64.